Current Chemistry Letters 15 (2026) 355–368

Contents lists available at GrowingScience

Current Chemistry Letters

homepage: www.GrowingScience.com

TD-DFT investigation of *N*,*N*-diphenylaniline-based organic dye adsorption on TiO_2 surfaces for dye-sensitized solar cells

Ahmed Arif[a,b], Badreddine Boukili[a,b*], Mohamed Kadour Atouailaa[b*], Ikram Mennas[b], El Mostafa Benharaf[b], Abdessamad Tounsi[a], Abdellah Zeroual[c] and Mohammed El idrissi[b]

[a]*Laboratory of Organic Chemistry, Catalysis and Environment. Faculty of Sciences. University Ibn Tofail. Kenitra, Morocco*
[b]*Team of Chemical Processes and Applied Materials, Sultan Moulay Slimane University, Polydisciplinary Faculty, Beni Mellal, 23000, Morocco*

C H R O N I C L E

Article history:
Received June 2, 2025
Received in revised form
June 27, 2025
Accepted January 2, 2026
Available online
January 2, 2026

Keywords:
DSSCs
TD-DFT
Photovoltaic performance
Open-circuit voltage
Electron injection energy

A B S T R A C T

Dye-sensitized solar cells (DSSCs) represent a highly promising new generation of photovoltaic devices that offer an attractive alternative to traditional silicon-based solar cells due to their low production costs, simple manufacturing, and adaptable optoelectronic properties. Titanium dioxide (TiO_2) is extensively utilized as a semiconductor in DSSCs due to the favorable position of its conduction band, high chemical stability, abundance, and non-toxicity. As part of this work, an in-depth computational study was conducted on five organic dyes (D1 to D5) to investigate their potential as effective sensitizers for DSSC applications. Density functional theory (DFT) and time-dependent DFT (TD-DFT) were employed to investigate their structural, electronic, and optical properties, as well as their key photovoltaic parameters. The HOMO energy levels calculated (−5.99 to −6.36 eV) were low enough to allow efficient dye regeneration by the electrolyte, while the LUMO levels (−3.05 to −3.71 eV) were located above the conduction band edge of TiO_2 (−4.0 eV), Calculated band gaps (2.35–2.94 eV) supported strong absorption in the visible range, and open-circuit voltages (0.26–0.94 eV) suggested good photovoltaic potential. Furthermore, all dyes presented positive free electron injection energy (ΔGinject), evidencing thermodynamically favorable charge transfer processes. Benchmarking revealed that structural modifications between dyes were found to be significantly.

© 2026 by the authors; licensee Growing Science, Canada.

1. Introduction

Dye-sensitized solar cells (DSSCs) are one of the most exciting third-generation photovoltaic technologies, enabling efficient converting of solar energy into electricity while keeping production costs low, ensuring high transparency, and facilitating easy production.[1] Since the groundbreaking work of Grätzel and O'Regan in 1991.[2] DSSCs have been the subject of constant attention and have undergone significant improvements in both design and efficiency. The basic structure of a DSSC consists of a transparent conductive oxide, a photoanode, a sensitizer dye, a redox electrolyte, and a counter electrode.[3] Among these components, the dye plays a central role, as it is responsible for capturing sunlight and activating charge separation by injecting photoexcited electrons into the semiconductor's conduction band.[4]

Titanium dioxide (TiO_2) is widely used as a photoanode material because of its high chemical stability, high availability, non-toxicity, and favorable conduction band position. Nevertheless, its large band gap (3.2 eV for anatase) limits its absorption principally to the ultraviolet region, representing only a minor fraction of the solar spectrum.[5] Therefore, the design of highly efficient sensitizing dyes displaying broad visible light absorption, adequate frontier orbital alignment, as well as strong electron injection capability remains a key technique for enhancing the performance of DSSCs. Organic dyes are particularly interesting because of their adjustable molecular structures, high molar extinction coefficients, and ease of synthesis about ruthenium-based complexes.[6] Donor-acceptor structures, in which electron-donating and electron-accepting groups are linked by π-conjugated bonds, have been shown to be especially efficient at promoting intramolecular charge transfer and expanding absorption in the visible range [7]**(Fig. 1).**

* Corresponding author
E-mail address motouailaa@gmail.com (M.K. Atouailaa) ikrammennas321@gmail.com (B. Boukili)
© 2026 by the authors; licensee Growing Science, Canada
doi: 10.5267/j.ccl.2026.1.002

A crucial factor affecting the efficiency of DSSCs is the relatif alignment of the dye's front molecular orbitals with the semiconductor and electrolyte. Effective dye-sensitized solar cells operate when the LUMO of the dye is situated above the conduction band of the TiO_2 to enable electrons to be injected freely, while the HOMO is below the redox potential of the electrolyte to allow the dye to be efficiently regenerated.[8] Furthermore, the injection free energy (ΔGinject) of electrons provides key information on the thermodynamic feasibility of electron transfer of the excited dye to the conduction band of TiO_2.[9]

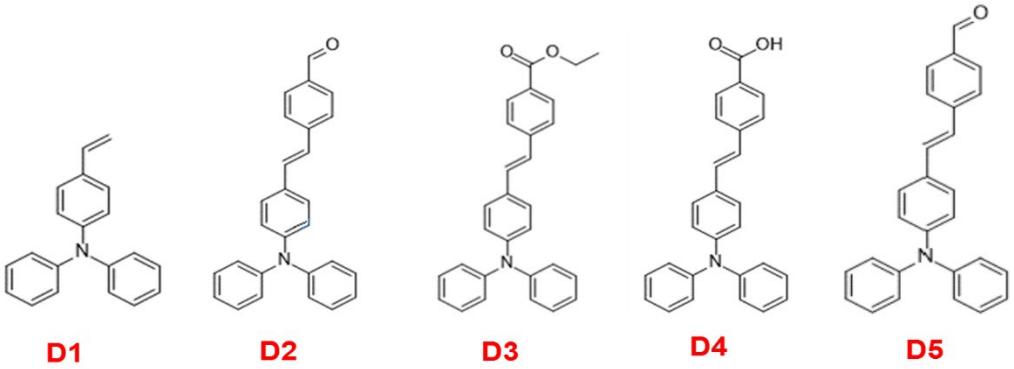

Fig. 1. Molecular structures of the five dyes (D1-D5).

In this framework, theoretical methods such as Density Functional Theory (DFT) and Time-Dependent Density Functional Theory (TD-DFT) are successful tools for the prediction of geometric, electronic, and optical properties of organic sensitizers.[10] In this paper, we have carried out computational research on five organic dyes (D1-D5) that are candidates for sensitization in DSSCs. These results enable an understanding of the relationships between structure and properties that influence dye performance and contribute to the rational design of new organic sensitizers for high-efficiency DSSCs.

2. Computational and validity methods

In this calculation, the different functions related to density functional theory (DFT), such as respectively ωB97XD[11], mPW1PW91[12], B3LYP[13], CAM-B3LYP[14], and B3PW91[15], are tested for dyes D1 to D5 using the 6-31G(d,p) basis set in order to select the most appropriate functional. The calculations are performed using the Gaussian 09 software package.[16-17]

In order to evaluate the reliability of the methods used to simulate optical properties, the theoretically calculated maximum absorption wavelengths were compared with the corresponding experimental values for dyes D1 to D5.[18] This comparison enables the reliability of the numerical approaches used to be estimated. As shown in **Scheme 1**, the B3LYP/6-31G(d,p) approach is distinguished by high accuracy in reproducing experimental data, which makes it the most relevant choice for the continuation of this investigation.

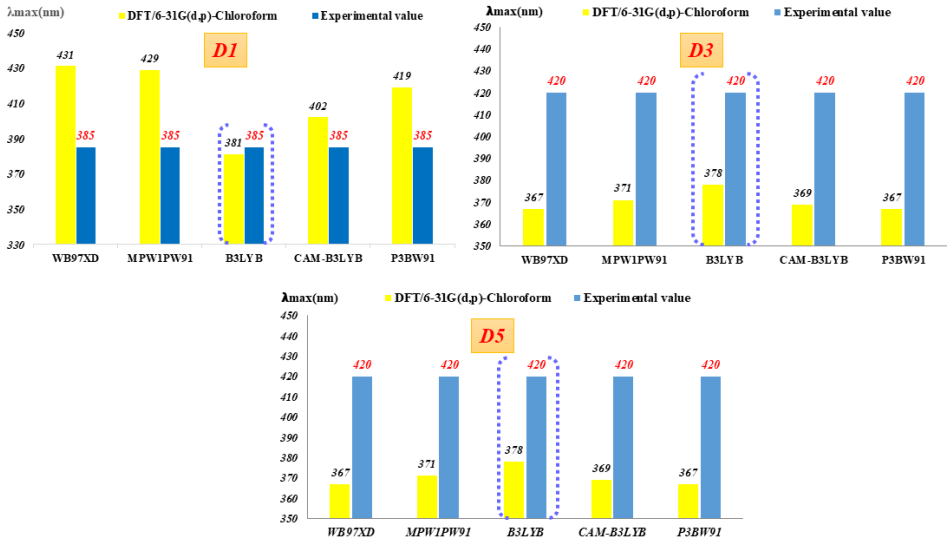

Scheme 1. Evaluation of the UV-Vis spectra of the dyes (D1, D2 and D5), simulated using the DFT method and compared with experimental data.

Scheme 2 plots the energies calculated using different DFT functionals, using the 6-31G(d,p) basis set. The results indicate that the B3LYP functional provides the lowest energy among all the functionals evaluated, thus attesting to the high stability of the dyes studied.[19-20] Based on this study, the B3LYP functional was selected as the most suitable for further studies. The structures of the designed dyes were then optimized by TD-DFT calculations with B3LYP. This method was also used for an in-depth exploration of their electronic and photovoltaic properties, again with the 6-31G(d,p) basis set, ensuring methodological consistency throughout the study.

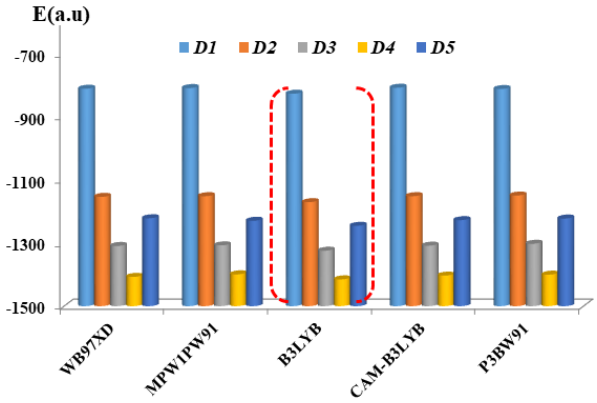

Scheme 2. Total energy of the different dyes (D1-D5) employing different functional in the TD-DFT.

The fundamental quantum and photoelectrochemical parameters were calculated based on the energies of the frontier orbitals (HOMO and LUMO) employing standard relationships from the literature. The band gap energy was calculated as the difference between the levels E_{LUMO} and E_{HOMO}. Chemical hardness and chemical potential were estimated from the electron affinity and ionization potential values, while molecular softness was derived from the ratio of the square of the chemical potential to the hardness. The electron affinity and ionization potential were derived from the energies E_{LUMO} and E_{HOMO} respectively, and the electronegativity was taken as the average of these two values. The open-circuit voltage (V_{OC}) was obtained from the difference between the level E_{LUMO} of the dye and the semiconductor conduction band border.[21]

$$Eg = E_{LUMO} - E_{HOMO} \quad (1)$$

$$\eta = \frac{I-A}{2} \quad (2)$$

$$\mu = \frac{(EHOMO + ELUMO)}{2} \quad (3)$$

$$\omega = \frac{\mu^2}{2\eta} \quad (4)$$

$$\chi = \frac{I + A}{2} \quad (5)$$

$$Voc = E_{LUMO} - E_{CB} \quad (6)$$

The different parameters calculated from the previous equations, including electron affinity (EA), ionization potential (IP), chemical potential (μ), chemical hardness (η), electronegativity (χ), flexibility (S), and electrophilicity (ω), were computed from the energies of the frontier orbitals and are reported in electron volts (eV). The corresponding values E_{LUMO} and E_{HOMO} correspond to the energy levels of the lowest and highest occupied molecular orbitals of the dyes studied, also expressed in eV. The results clearly demonstrate that the B3LYP functional has the lowest energies among all the methods tested, confirming the structural stability of the dyes[2]. After the most suitable functional was identified, the TD-DFT/B3LYP method was used for the detailed study of the optical, electronic, and photovoltaic properties of the dyes, using the same 6-31G(d,p) basis set to ensure methodological consistency across all calculations.

3. Results and discussions

3.1. Analysis of Molecular Frontier Orbitals

Quantum chemistry methods, in especially density functional theory (DFT) and its time-dependent version (TD-DFT), are strong tools for probing the structural configuration and electronic performance of organic dyes, in the ground state as in the excited state. In this study, five organic dyes (D1-D5) were explored to determine their potential as sensitizers for dye-sensitized solar cells (DSSCs). The fundamental state-optimized geometries, achieved at the B3LYP/6-31G(d,p) level, are illustrated in **Fig.2** These optimized structures have been subsequently used as a basis for calculating electronic and optical properties, providing in-depth explanations of the structure-property relationships that affect the photovoltaic performance of these systems.[23-24]

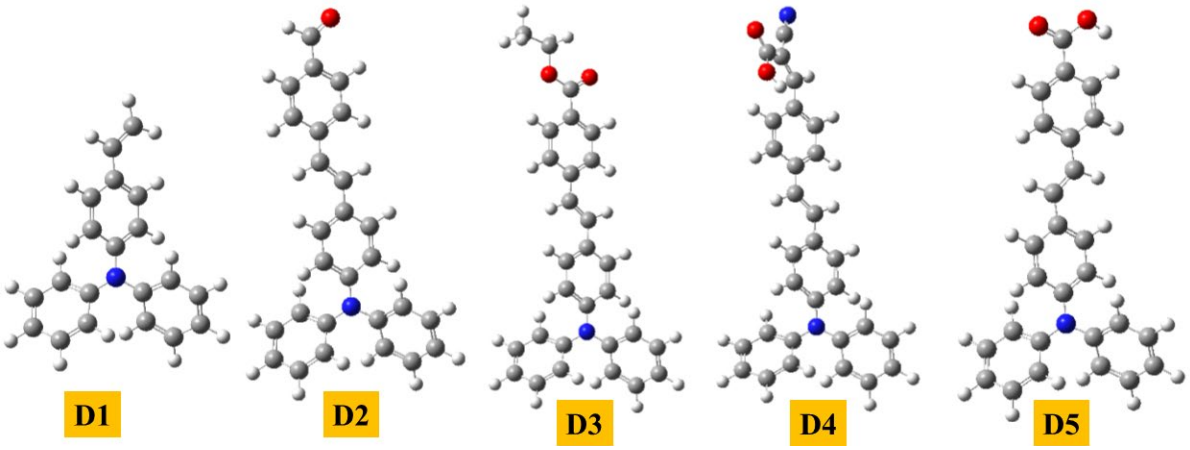

Fig. 2. Optimization of the ground state geometry of the dyes (D1-D5) studied with the B3LYP/6-31G (d,p) level.

The HOMO and LUMO molecular orbital distributions of the dyes studied are plotted in **Fig.3,** on the basis of the B3LYP/6-31G(d,p) theoretical level. The investigation of optimized geometries, functional group orientation, and charge transfer performance provides crucial insights into electronic interactions and enhances the potential of these dyes as exciting sensitizers for dye-sensitized solar cells.[25-26]

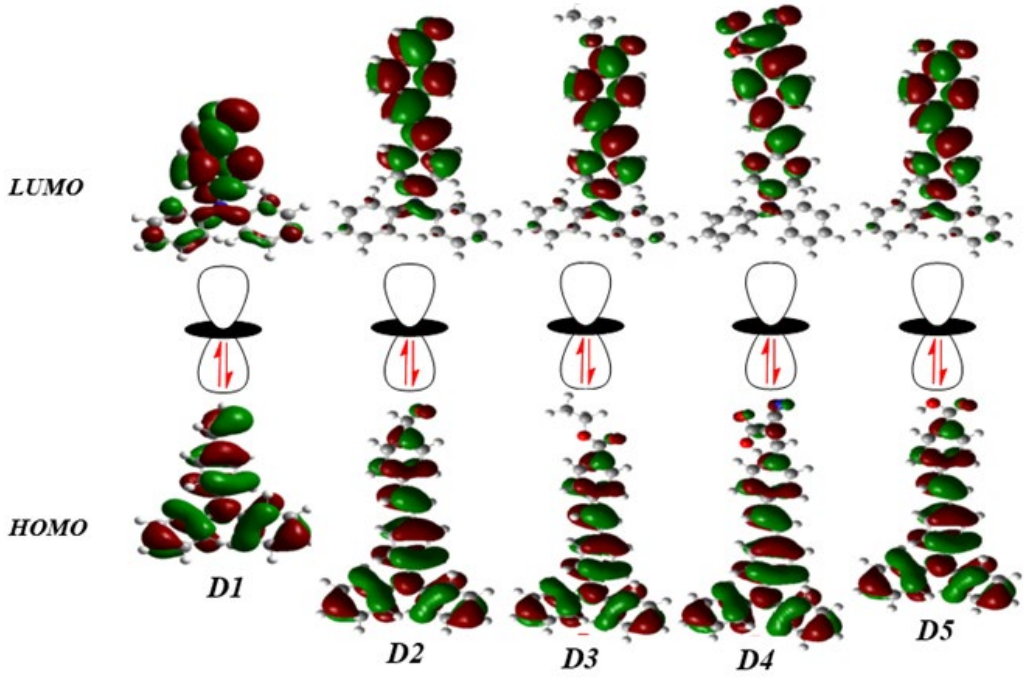

Fig. 3. HOMO and LUMO molecular orbital diagrams for the dyes (D1-D5) examined.

3.2. Electronic Proprieties

Table 1 summarizes the main quantum chemical parameters, including the energy gap (Egap), chemical potential (μ).

Table.1. Calculated Frontier Molecular Orbital Energies and Band Alignment of Dyes D1–D5 with TiO_2.

Dyes	E_{HOMO}	E_{LUMO}	E_{Gap}	μ	E_{0-0}	*CBOP* $E_{VB} + E_{0\text{-}0}$
D1	-6.00	-3.06	2.94	-4.53	4.03	-1.96
D2	-6.09	-3.73	2.36	-4.91	3.25	-2.84
D3	-6.02	-3.53	2.49	-4.77	3.30	-2.71
D4	-6.37	-3.60	2.77	-4.98	2.81	-3.55
D5	-6.16	-3.71	2.45	-4.93	3.27	-2.88
TiO_2	**-7.16**	**-4**	**3.2**	**-5.6**	**	**

The calculated electronic properties of dyes D1–D5, together with reference values for the TiO_2 semiconductor and the electrolyte, are summarized. For dye D1, the HOMO and LUMO energy levels are −6.00 eV and −3.06 eV, respectively, yielding an energy gap (Egap) of 2.94 eV, an optical transition energy ($E_{0–0}$) of 4.03 eV, and an excited-state oxidation potential (CBOP) of −1.96 eV. Dye D2 exhibits EHOMO = −6.09 eV, ELUMO = −3.73 eV, Egap = 2.36 eV, E0−0 = 3.25 eV, and CBOP = −2.84 eV. For dye D3, the values are EHOMO = −6.02 eV, E_{LUMO} = −3.53 eV, E_{gap} = 2.49 eV, E0−0 = 3.30 eV, and CBOP = -2.71 eV. Dye D4 shows E_{HOMO} = −6.37 eV, ELUMO = −3.60 eV, Egap = 2.7704 eV, E0−0 = 2.8140 eV, and CBOP = −3.5558 eV. Finally, dye D5 presents EHOMO = −6.16 eV, ELUMO = −3.71 eV, Egap = 2.45 eV, E0−0 = 3.27 eV, and CBOP = −2.88 eV. The chemical potential (μ) of the dyes extends to between -4.5262 and -4.9846 eV, indicating broadly similar electronic properties and favorable compatibility for electron transfer from the dyes to the conduction band of TiO_2. Such values are being analyzed in comparison with the energy levels of the TiO_2 semi-conductor, the valence band of which is positioned at −7.16 eV, the conduction band at −4.00 eV, with a band gap of 3.20 eV, and an electrolytic redox potential of −5.60 eV.

These investigations demonstrate clearly that the LUMO energy levels of all dyes are positioned over the limit of the TiO_2 conduction band, while their HOMO levels are below the redox potential of the electrolyte. This energy -positioning allows for efficient injection of electrons from the activated dyes into the conduction band of TiO_2, as well as efficient recovery of the dyes by the electrolyte. Furthermore, the relatively small energy gaps observed for dyes D2, D3, and D5 suggest better light absorption and charge transfer characteristics. Accordingly, these dyes, particularly dyes D2 and D5, exhibit electronic configurations that are attractive for efficient photovoltaic performance in dye-sensitized solar cells (DSSCs).

3.3. Molecular Electrostatic Potential (MEP)

Molecular electrostatic potential (MEP) analysis is a useful tool for visualizing the distribution of charge density on the surface of molecules, thereby identifying reactive sites that are likely to interact with electrophilic or nucleophilic substances. This method provides a clear three-dimensional representation of regions with high or low electron density, facilitating the understanding of intermolecular interactions, particularly in the context of dye adsorption on the surface of the TiO_2 semiconductor.[27] The MEP surfaces of the five dyes studied (D1 to D5) are simulated and presented as potential maps in **Fig.4.**

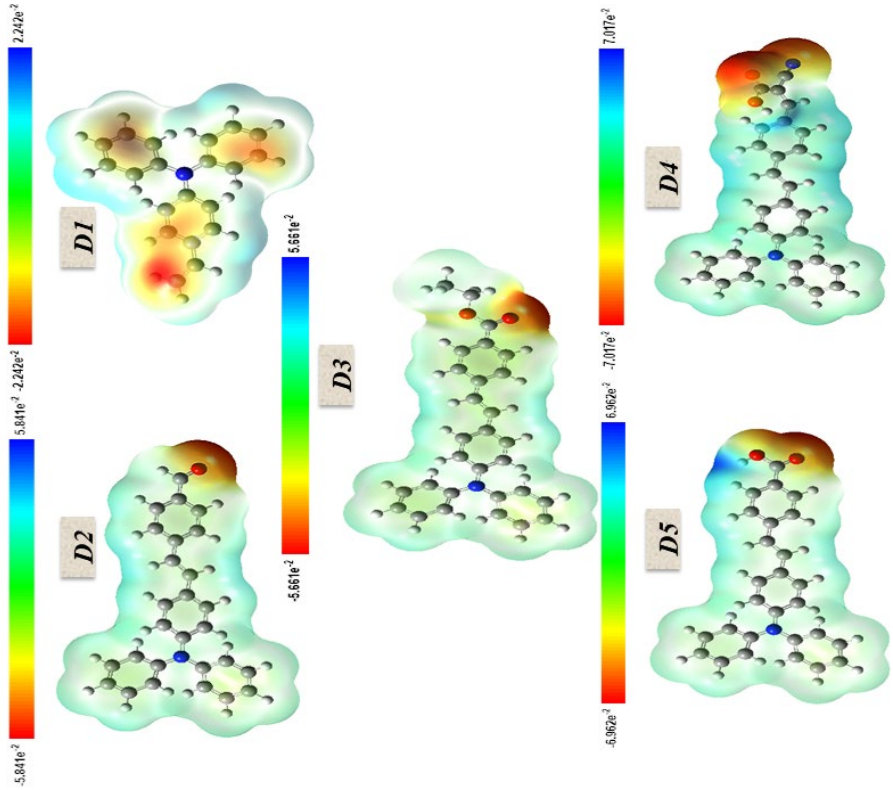

Fig. 4. Maps of molecular electrostatic potential of dyes D1–D5, performed at B3LYP/6-31G(d,p) level

The molecular electrostatic potential (MEP) of dyes D1 to D5 shows a high localized electron density on a side group for D1, suggesting a strong polarization favorable to charge transfer to TiO_2, while D2 exhibits a negative charge accumulation on a carbonyl or methoxy group, facilitating selective adsorption and electron transfer. D3 is distinguished by a more homogeneous distribution, indicating a balanced charge, which is potentially beneficial for stability but less optimal for directional polarization. Dyes D4 and D5 have symmetrical red areas at the ends and a more electropositive or

neutral center, promoting oriented intramolecular charge transfer, which improves photoelectrochemical efficiency and electron transfer directionality, essential for the performance of dye-sensitized solar cells.[28]

3.4. Density of States (DOS)

The analysis of total and partial density of states (DOS) spectra is an important step in understanding the electronic properties of molecular dyes. In this work, we analyze the DOS spectra of dyes D1 to D5 in order to evaluate the distribution of electronic energy levels and their contribution to optical transitions.[29] This approach provides a better insight into interactions between molecular orbitals and enables the identification of dominant electronic states responsible for the specific optoelectronic properties of the dyes, as illustrated in **Fig.5.**

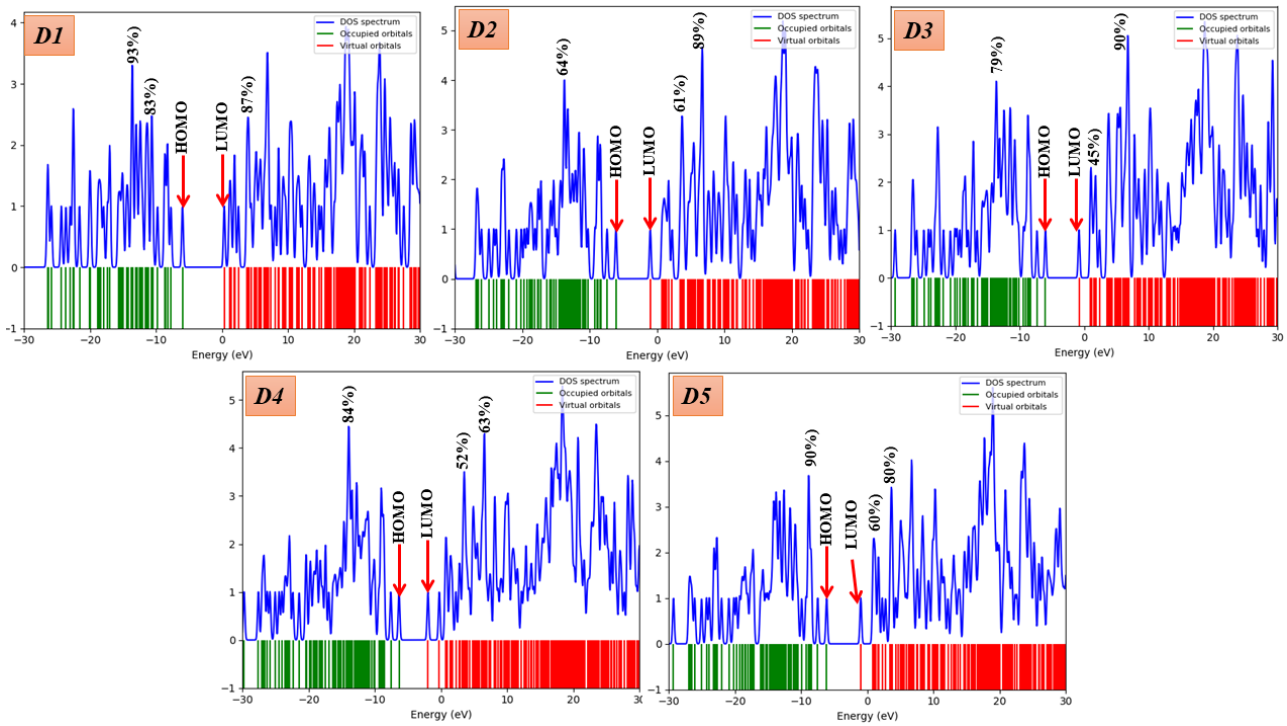

Fig. 5. Total and Partial Density of States (DOS) Spectra of Dyes D1–D5

The present measurement indicates that the dyes D4 and D3 also exhibit significant donor character, with respective contributions of 84% and 79% to the molecular energy level (HOMO), and a notable contribution to the molecular energy level (LUMO), indicating significant participation in frontier molecular orbitals. Furthermore, dyes D4 and D3 also exhibit a very pronounced donor character, with respective contributions of 84% and 79% to the HOMO, accompanied by a slight contribution to the LUMO, suggesting a certain degree of electron delocalization between the donor and acceptor fragments. In contrast, dye D2 is distinguished by a more moderate contribution to the HOMO (64%) and an almost negligible contribution to the LUMO (0.1%), reflecting a spatially decoupled donor character, with a clear separation between donor and acceptor orbitals, thus minimizing electronic interactions at the LUMO level.[30]

3.5. UV-VIS Absorption Properties

The modeled UV-Vis absorption spectra of dyes D1 to D5, obtained using B3LYP/6-31G(d,p) modeling, are plotted in **Fig. S1**. All the dyes possess a significant absorption band between 270 and 380 nm, which corresponds to the main π→π* transition of the HOMO→LUMO type. The spectral properties correlate with the molecular structure: dyes D3 and D4 exhibit stronger, red-shifted absorptions, which is characteristic of efficient intramolecular charge transfer and higher light-harvesting properties. Conversely, the blue-shifted absorptions of dyes D1 and D2 are consistent with their larger energy gaps. Overall, these results highlight the very clear structure-property relationship, identifying D3 and D4 as the most effective sensitizers in the series due to their superior optical absorption profiles, which are essential for high-performance DSSCs.[31-32]

D-DFT calculated the UV-Vis absorption spectra of dyes D1 to D5, revealing distinct absorption bands in the ultraviolet to visible region (200-400 nm), corresponding primarily to π→π∗ electronic transitions. Dye D3 has the highest and most red-shifted absorption maximum, suggesting enhanced light-harvesting ability and more extensive conjugation in the molecular structure. Similarly, dyes D4 and D5 exhibit broad profiles extending to greater wavelengths, which suggests improved charge transfer properties. Conversely, dyes D1 and D2 exhibit relatively blue-shifted and lower-intensity peaks, indicating

less extensive conjugation and weaker electron delocalization. These spectral differences clearly indicate the powerful interaction of molecular substitution on the electronic transitions and optical characteristics of the dyes. Overall, the exceptional absorption characteristics of dyes D3 and D5 make them promising candidates for efficient photon capture in dye-sensitized solar cell (DSSC) applications.

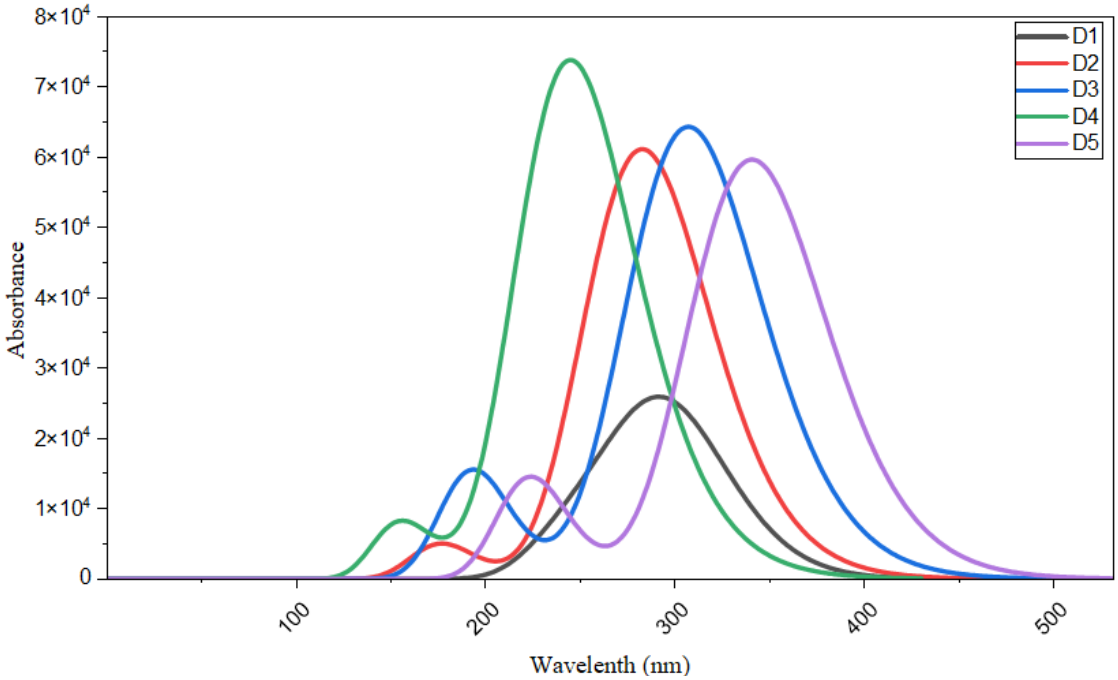

Fig. 6. UV–Vis Absorption Spectra of Dyes D1–D5 Calculated by TD-DFT

Indeed, the structure of the dye molecule contains electron-accepting units that facilitate intramolecular charge transfer, resulting in distinct absorption peaks in UV-Vis spectra[33]. Structural changes therefore seem to improve the performance of DSSCs by increasing their absorption of light. Furthermore, the strongest oscillation force is associated with the transition from the electronic ground to the excited state. The modified compounds' absorption spectra are shown in **Fig.6**.

3.6. Photovoltaic Properties

The energy -difference between the LUMO level of the acceptor and the HOMO level of the donor defines the open-circuit voltage (Voc) of a DSSC.[34] The calculated electronic properties of dyes D1–D5 are summarized in the **Table** 2. The values of E_{HOMO} and E_{LUMO} vary from –6.00 to –6.37 eV and also from -3.60 to –3.71 eV, indicating good electronic stability of the dyes. The energy gap (Egap) ranges from 2.36 to 2.94 eV, suggesting efficient absorption in the visible region. The open-circuit voltage (V oc) values range from 0.27 to 0.94 eV, suggesting a favorable capacity for electron transfer to the TiO_2 conduction band (-4.0 eV)[34]. The negative nature of the free injection energy (ΔG inject), varying between –0.44 and -2.04 eV, supports the spontaneity of electron transfer from the LUMO of the dyes to the conduction level of the semiconductor. These results indicate excellent combination energy between the dyes and TiO_2, an indispensable condition for efficient separation and transport of photoinduced charges. These dyes consequently show promising potential for applications in dye-sensitized solar cells (DSSCs).

$$\Delta G^{inject} = E^{dye*} - E_{CB} \tag{7}$$

where E_{CB} represents the conduction band of TiO_2, and E^*_{dye} corresponds to the oxidation potential of the excited organic dye, as defined by Equation[35]:

$$E^{dye*} = E_{Dye} - E_{00} \tag{8}$$

where in this equation, E_{dye} corresponds to the oxidation potential of the dye in its ground state (related to E_{HOMO}), while E_{00} represents the energy of the vertical electronic transition related to the absorption maximum.

Table 2. Photovoltaic Parameters and Frontier Orbital Energies and of the Dyes Relative to TiO_2

Dye	E_{HOMO}	E_{LUMO}	E_{gap}	V_{oc}	ΔG^{inject}
D1	-5.99	-3.06	2.94	0.94	-2.04
D2	-6.09	-3.73	2.36	0.27	-1.16
D3	-6.02	-3.53	2.49	0.47	-1.28
D4	-6.37	-3.6	2.77	0.40	-0.44
D5	-6.16	-3.71	2.45	0.29	-1.12
TiO_2	**-7.16**	**-4.00**	**3.20**	**-5.60**	***

All dyes exhibit negative ΔG^{inject} values, confirming that electron injection into TiO_2 is thermodynamically favorable. D1 has the most negative ΔGinject value (-2.04 eV) and the highest open-circuit voltage (Voc) (0.94 eV), indicating a strong driving force and efficient photovoltage generation. In contrast, D4 has a less negative ΔGinject (-0.44 eV), indicating a weaker injection force but higher structural stability. D3 has balanced characteristics between energy alignment and electron transfer capacity. Overall, D1 emerges as the most promising sensitizer, followed by D3, with both sensitizers offering an optimal balance between absorption efficiency, injection potential, and photovoltaic performance.

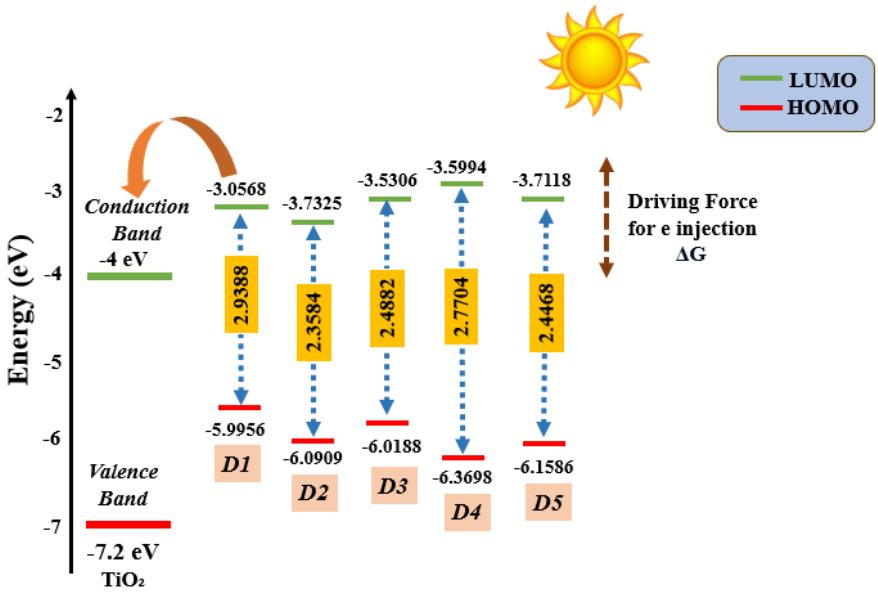

Fig.7. Energy levels of the dyes investigated (D1, D2, D3, D4 and D5).

The energy levels and electron injection process for dyes D1 to D5 at the TiO_2 semiconductor interface are plotted in **Fig.7**. The HOMO and LUMO energy levels of the dyes are illustrated by red and green bars, respectively, while the ELUMO and EHOMO levels of TiO_2 are positioned at –4.0 eV and –7.2 eV. The diagram shows that the LUMO level of all dyes is above the conduction band of TiO_2, a condition that favors electron injection after photoexcitation in a thermodynamically favorable manner. On light absorption, an electron is moved from the dye's HOMO to its LUMO, then injected into the conductivity band of TiO_2. Dyes D1 and D3, featuring higher LUMO levels, favor more efficient electron injection. All the dyes show good regeneration and suitable energy alignment for DSSCs, with D1 and D3 being the most successful candidates. The oscillator strength parameter f, at the wavelength of maximum absorption (λmax), is used to calculate LHE according to:

$$LHE = 1 - 10^{-f} \quad (9)$$

The values of LHE obtained are shown in the **Table 3**, and range from 0.741 to 0.984. The dyes D3 and D4 exhibit the greatest values (0.974 and 0.984), indicating a high capacity for light absorption and improved efficiency in generating photoelectrons. suggesting that the incorporation of conductive groups significantly enhances photocurrent generation.[36-37]

Table 3 shows the principal electronic transitions for dyes D1 to D5, calculated by TD-DFT. Excitation energies, their corresponding wavelengths, oscillator strengths (f), and prevailing orbital contributions are included. For all dyes, the strongest absorption bands are in the UV-visible region (270–440 nm). Such bands are attributed mainly to π→π∗ transitions involving the HOMO and LUMO orbitals or their close neighbors.

Dye-1: The strongest transition occurred at 307 nm (f = 0.5876) and was primarily due to HOMO → LUMO excitation. Further transitions at 275 and 267 nm were indicative of HOMO → L+1 and HOMO → L+2 contributions.

Dye-2: Exhibits high absorption at 381 nm (f = 1.5091), which is also characterized by the HOMO → LUMO transition, which suggests efficient light capture in the near-UV region.

Dye-3: This dye has a similar performance, with an intensive band at 375 nm (f = 1.5876), while lower transitions can be seen between 276 and 271 nm.

Dye-4: Characterized by the lowest energy transition of the dyes examined, with strong absorption at 440 nm (f = 1.822). This absorption extends further in the visible region, which indicates that D4 could enable better utilization of sunlight than other dyes.

Dye-5: The principal absorption maximum of this dye is at 378 nm (f = 1.472), which is consistent with a strong HOMO → LUMO transition, while weaker absorptions occur at shorter wavelengths.

Table 3. Excitation energy E_{EX}, absorption wavelength (λ), oscillator strength (f), light-harvesting efficiency (LHE), and main electronic transitions of dyes D1–D5 calculated using TD-DFT.

Dyes	*Eex(eV)*	*λ (nm)*	*f*	*LHE*	*Transition*
	4.03	307	0.588		H → L (93%)
D1	4.50	275	0.169	0 .741	H → L_{+1} (87%)
	4.63	267	0.031		H → L_{+2} (83%)
	3.25	381	1.509		H → L (89%)
D2	3.72	333	0.0001	0.969	H_{-1} → L (64%)
	4.49	275	0.124		H → L_{+1} (61%)
	3.30	375	1.588		H → L (90%)
D3	4.49	276	0.121	0.974	H → L_{+2} (44%)
	4.56	271	0.266		H_{-1} → L (79%)
	2.81	440	1.822		H→ L (84%)
D4	3.90	317	0.146	0.984	H_{-1} → L (60%)
	3.98	311	0.059		H_{-6} → L (52%)
	3.27	378	1.472		H → L (90%)
D5	4.50	275	0.109	0.966	H → L_{+2} (60%)
	4.55	272	0.251		H_{-1} → L (80%)

3.7. Charge Transport and Charge Transfer

The integral charge transfer (t) is a fundamental element in determining charge transport within dyes. This is a parameter of the dimensional configurations that is strongly influenced by frontier molecular orbitals (FMOs). This factor is defined by the equation from Koopman's theorem.[38]

$$\mathbf{t_{electron}} = \frac{\mathbf{1}}{\mathbf{2}}(\mathbf{E_{LUMO+1}} - \mathbf{E_{LUMO}}) \quad (10)$$

$$\mathbf{t_{hole}} = \frac{\mathbf{1}}{\mathbf{2}}(\mathbf{E_{HOMO}} - \mathbf{E_{LUMO-1}}) \quad (11)$$

The rearrangement energy is made up of two contributions: internal (λ_{int}) related to structural changes in the molecule, and external (λ_{ext}) due to the environment. As the effect of the surroundings on electron mobility is negligible, only λint is taken into account in this study. Hence, the reorganization energies of holes (λ_h) and electrons (λ_e) are calculated from the following equation.[34]

$$\boldsymbol{\lambda_e} = [\boldsymbol{E_0^{anion}} - \boldsymbol{E^{anion}}] + [\boldsymbol{E_0^{anion}} - \boldsymbol{E_0}] \quad (12)$$

$$\boldsymbol{\lambda_{hol}} = [\boldsymbol{E_0^{cation}} - \boldsymbol{E^{cation}}] + [\boldsymbol{E_0^{cation}} - \boldsymbol{E_0}] \quad (13)$$

These internal reorganization energies correspond respectively, figto the transfer of electrons and holes, as follows:

- E_0: Energy of the neutral molecule in its optimized geometry
- E^{anion}, E^{cation}: Energies of optimized anion and cation geometries
- E_0^{anion}, E_0^{cation} : Energies of anion/cation computed at the neutral geometry

The following equation expresses the appropriate formula for K_{CT} in the absence of a barrier [39]:

$$\boldsymbol{k_{CT}^{hol/elec}} = \left(\frac{\boldsymbol{\pi}}{\boldsymbol{\lambda^{hol/elec} k_B T}}\right)^{1/2} \frac{\boldsymbol{t_{hol/elec}^2}}{\boldsymbol{h}} \boldsymbol{e}^{\left(\frac{\lambda^{hol/elec}}{4k_B T}\right)} \quad (14)$$

With k_B as the Boltzmann constant, t as an electronic coupling matrix across two molecules, T as the temperature on an absolute scale (298 K) with h as the reduced Planck constant, k_{CT} depends primarily on both the charge transfer integral and the reorganization energy.

Table 4. On the TD-DFT B3LYP/6-31G(d,p) Level, Charge Transport Rates and Transfer of Charge Integrals were Calculated for Every Dye.

	t_{hol}	$t_{electron}$	λ_{hol}	$\lambda_{electron}$	k_{CT}^{hol}	$k_{CT}^{electron}$
D1	0.8778	0.965	0.5187	0.3046	$1.152*10^{14}$	$1.459*10^{15}$
D2	0.6623	1.497	0.874	0.5423	$1.593*10^{12}$	$2.613*10^{14}$
D3	0.6656	1.2803	0.7004	0.473	$9.720*10^{12}$	$4.006*10^{14}$
D4	0.6081	0.6707	0.6234	0.4085	$1.822*10^{13}$	$2.218*10^{14}$
D5	0.6637	1.4268	0.7834	0.5006	$4.066*10^{12}$	$3.698*10^{14}$

The efficiency of charge transport in photovoltaic power systems is determined by the interactions between the electron coupling (t) and the reorganization energy (λ). Higher charge transfer, which minimizes recombination losses, is achieved with greater coupling and lower reorganization energy. In the series of dyes examined, we consistently observe a trend whereby the electron reorganization energy (λ_e), ranging from 0.305 to 0.543 eV, consistently lower than the hole reorganization energy (λ_h), which ranges between 0.519 and 0.874 eV. Consequently, the electron transfer rate is significantly higher, ranging from 2.22. 10^{14} to 1.46. 10^{15} s^{-1}, compared to the hole transfer rate, which ranges from 1.59. 10^{12} to 1.15. 10^{14} s^{-1}.

Dye D1 emerges as the superior candidate, exhibiting the fastest electron transfer rate ($\boldsymbol{k_{CT}^{electron}} \approx 1.46 \times 10^{15}$ s^{-1}). This exceptional performance is attributed to an optimal combination of the lowest electron reorganization energy (λe = 0.3046 eV) and strong electronic coupling ($\mathbf{t_{ele}}$ =0.965 eV). Furthermore, D1 also displays the most efficient hole transfer ($\boldsymbol{k_{CT}^{hol}}$ = $1.15 \times 10^{14} s^{-1}$) due to its minimal hole reorganization energy ($\boldsymbol{\lambda_{hol}}$ = 0.5187 eV).The general ranking of electron transfer performance is D1 ≫ D3 > D5 > D2 > D4, based on the balance between telectrons and $\boldsymbol{\lambda_{electron}}$. For hole -to-hole transfer, the ranking is D1 > D4 > D3 > D5 > D2, with the high performance of D2 being significantly hampered by its very large $\boldsymbol{\lambda_{hol}}$ (0.874 eV) despite its strong coupling. These patterns suggest that, although all dyes are engineered to promote the rapid electron migration required for n-type semiconductors such as TiO_2, D1 is overall the most promising candidate for minimal charge transport losses and maximized photocurrent power generation.

4. Adsorption of dyes on (TiO_2) cluster

The investigation of dyes adsorbed on TiO_2 -based complexes is crucial for dependably evaluating their optoelectronic properties and performance in dye-sensitized solar cells (DSSCs). The dye adsorption on the TiO_2 surface takes on a crucial function in modulating its electronic properties. In order to give an early qualitative characterization of the interactions occurring between the dye and the oxide, the (TiO_2) cluster model was employed. The optimized structures of the dye-TiO_2 complexes were derived from ab initio calculations based on density functional theory (DFT), a broadly used approach for investigating molecular systems and materials at the atomic scale. These computations were conducted using the DMol³ code, embedded in the Materials Studio software, providing advanced tools for molecular modeling and materials simulation.[40]

Geometric optimisations were performed in the context of generalised graphite abstraction (GGA), based on the Perdew-Burke-Ernzerhof (PBE) functional,[41] known for its in-depth description of electronic interactions in semiconductor-type systems. Furthermore, in order to maintain a high level of accuracy in electronic structure studies, the double numerical basis set with polarisation functions (DNP) was adopted. This offers an optimal balance between accuracy and computational efficiency, which is particularly interesting for studies of complex and large-scale systems. The adsorption energy $\mathbf{E_{ads}}$ of the dyes on the $(TiO_2)_8$ clusters was then evaluated using the following equation:

$$\boldsymbol{E_{ads} = E_{Dye\text{-}TiO2} - (E_{Dye} + E_{TiO2})} \quad (15)$$

E_{dye/TiO_2} represents the total energy of the adsorbed compound, E_{Dye} represents the energy of the separated dye, and E_{TiO_2} represents the energy of the bare TiO_2 cluster. This energy provides a quantitative indication of the stability of adsorption and the strength of interactions between the dye and the TiO_2 surface, two key factors in the selection and optimisation of innovative photosensitiser materials for DSSCs. A higher negative adsorption energy value means a stronger bond strength and better stability of the dye-semiconductor interface.[42]

The adsorption energies of dyes D1 to D5 on TiO_2 reveal significant differences in terms of stability. Indeed, the more negative the energy value, the stronger the interaction and the more stable the adsorption. Dye D4 has the lowest adsorption energy (-3.169 eV), which means it has a strong affinity for TiO_2, while dye D1 has the highest value (-1.045 eV), indicating a weaker interaction. The descending order of affinity is therefore as follows: D4 > D3 > D2 > D5 > D1.

In DSSC applications, an effective dye must combine strong adsorption with the possibility of controlled desorption. D4 therefore appears to be the most promising candidate, subject to further study of its electronic properties. As all the values observed are negative, the adsorption process is spontaneous and thermodynamically favourable. These results confirm the potential of these dyes for photovoltaic applications.

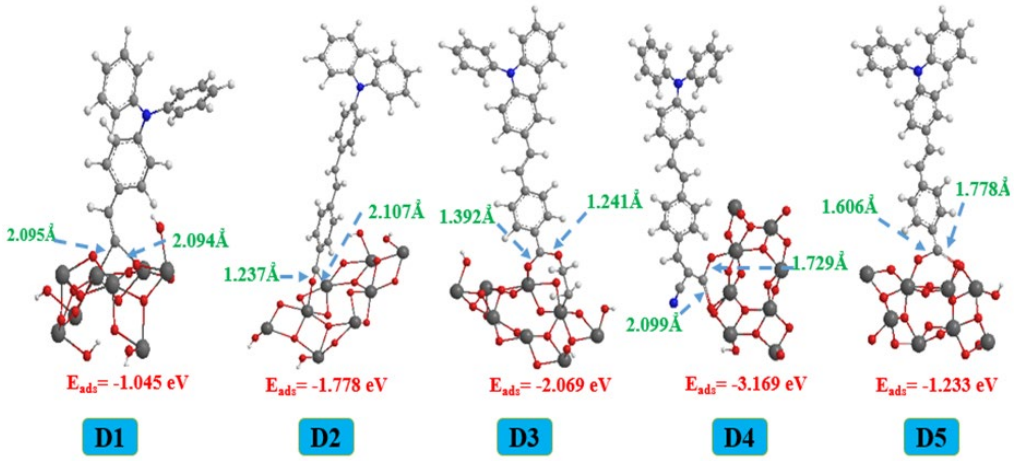

Fig. 8. Ground-state optimized structures of all dyes with TiO_2

4.1. Anchoring dyes onto ($(TiO_2)_8$ cluster

The stability of the orbital energies of dyes adsorbed on TiO_2 differs considerably from that observed for free dyes. Indeed, as shown in **Table 5** (**Fig. 9**), the values of the E HOMO and E LUMO levels differ depending on the nature of the dye, reflecting different degrees of interaction with the semiconductor surface. This interaction causes partial destabilization of the HOMO level depending on the charge transfer between the dye orbitals and the Ti(IV) ions on the surface. It can be seen that the energies *E* LUMO E LUMO of the Dn@TiO₂ systems remain relatively similar to those of the free dyes, while the band gaps (E gap) are generally smaller after adsorption, as a result of the HOMO level shifting to lower values. This narrowing of the band promotes electron transfer and improves the ability to inject electrons from the energized LUMO into the conduction band of TiO_2. Among the complexes studied, D3@TiO₂ has the smallest band gap Egap, which means better absorption of visible light and potentially higher efficiency in the photovoltaic conversion process.

Table 5. Value of energy HOMO, LUMO and E_{gap} for all Dye adsorbed to TiO_2

Dye	E_{HOMO}	E_{LUMO}	E_{gap}
D1@TiO₂	-4.7695	-2.6642	2.1053
D2@TiO₂	-5.7322	-3.4394	2.2928
D3@TiO₂	-4.8168	-3.0008	1.816
D4@TiO₂	-6.1739	-2.9015	3.2724
D5@TiO₂	-5.4201	-2.7904	2.6297

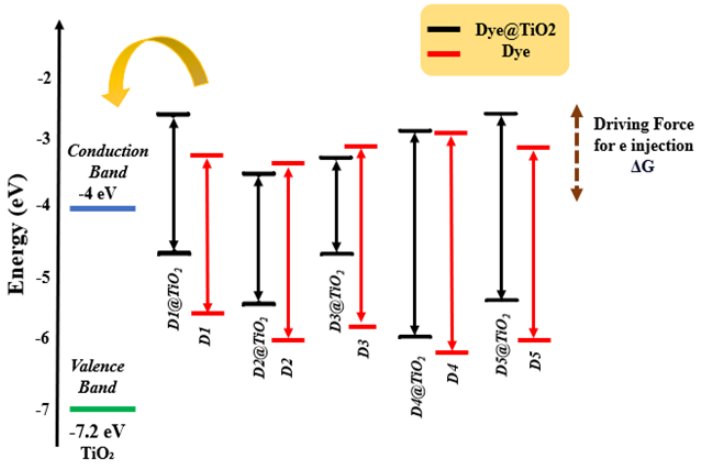

Fig. 9. Energy Level Alignment and Electron Injection Driving Force (ΔG) of Dyes D1–D5 and Their Complexes with TiO_2

Fig. 9 shows the alignment of the energies of the frontier molecular orbitals (HOMO and LUMO) of dyes D1 to D5 and their corresponding dye@TiO₂ complexes with respect to the conduction and valence bands of TiO_2. The red bars indicate the isolated dyes, while the black bars correspond to the dyes adsorbed on TiO₂. The conduction band (−4.0 eV) and valence band (−7.2 eV) of TiO_2 serve as reference levels. In the case of complexation, the HOMO and LUMO energy levels of the

dyes shift towards stabilisation, confirming the strong electronic interaction and charge delocalisation at the dye-semiconductor interface.

The LUMO levels of all dyes are located above the conduction band of TiO_2, which guarantees thermodynamically favourable electron injection (negative ΔG) from the excited dye to TiO_2 after photoexcitation. Conversely, the HOMO levels are above the valence band of TiO_2, ensuring efficient dye regeneration by the electrolyte. Among all the systems studied, D3 and D5 have the most optimised energy configuration, offering the greatest driving force for electron injection and HOMO levels suitable for rapid regeneration. This energy configuration explains their expected superior performance in terms of light capture and photovoltaics in dye-sensitised solar cells.

4.2. HOMO-LUMO density analysis

The binding of the dye to the surface is crucial for the quality and durability of dye-sensitised solar cells[43]. Due to their superior optoelectronic characteristics, which enable the efficient generation and transfer of free electrons and holes as well as a higher expected open-circuit voltage (V_{OC}), dyes D1, D2, D3, D4, and D5 are the focus of this section. We turned to the $(TiO_2)_8$ cluster,[44] which offers balanced electronic characteristics, to illustrate the surface of the TiO_2 semiconductor.

The HOMO and LUMO distributions of all dye-TiO_2 compounds[8] are illustrated in **Fig.10**. This clearly shows that the HOMOs are mainly located on the D-A-D structure of the dye, while the LUMOs are dispersed over the entire surface of the TiO_2 semiconductor.[8] This indicates the availability of intermolecular charge transfer between the dyes and TiO_2.

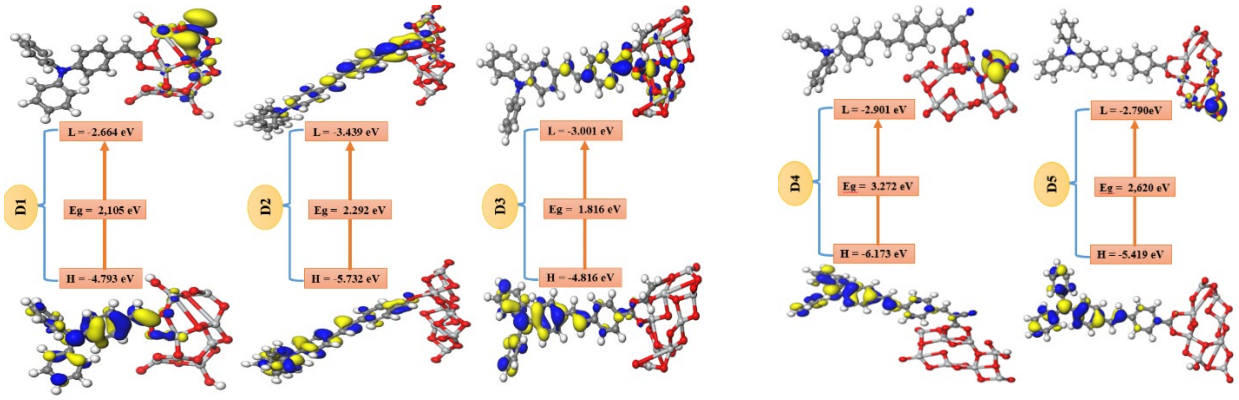

Fig.10. Simulated frontier molecular orbitals of dye-$(TiO_2)8$ cluster obtained using DMol3

Frontier molecular orbital (FMO) testing of dyes D1 to D5 adsorbed on TiO_2 shows effective electronic pairing between the dyes and the semiconductor surface. In our complexes, the HOMO orbits are mainly localized on the donor or π-conjugated regions, while the LUMO orbits stretch towards the anchoring groups and TiO_2- clusters, indicating a favorable direction of charge transfer upon photoexcitation. The HOMO energy levels range from −4.79 to −6.17 eV and the LUMO levels from −2.66 to −3.44 eV, leading to band gaps (Eg) between 1.82 and 3.27 eV.Among them, D3@TiO_2 exhibits the smallest band gap (1.816 eV) and optimal alignment of its LUMO (−3.00 eV) with the TiO_2 conduction band (−4.0 eV), favoring efficient electron injection and broad visible-light absorption. In contrast, D4@TiO_2 shows the widest gap (3.27 eV), suggesting lower optical activity. The electron density distributions confirm that photoinduced charge transfer occurs from the dye's aromatic donor moiety toward the TiO_2 surface through the anchoring groups, validating the donor–π–acceptor design. In any case, the energy alignment and orbital delocalisation indicate that dye adsorption effectively enhances interfacial charge transfer, making D3@TiO_2 most promising sensitiser for high-efficiency dye-sensitised solar cells (DSSCs). Hence, this work can be considered as strong evidence for the importance of applied chemical sciences in different fields, as previously reported.[45–51]

5. Conclusion

Theoretical DFT and TD-DFT studies have provided a precise roadmap for the rational design of super-powerful organic dyes. The study revealed that even though all compounds (D1-D5) met the electron injection energy requirements in TiO_2, the performance of the system depends on the critical balance between the dynamics of photon capture and those of dye electrolyte regeneration. While adsorption leads to a reduction in the E band gap and a redistribution of electron density, confirming strong interfacial coupling, an excessively high HOMO, as in D3@TiO_2, can jeopardise regeneration despite good light harvesting efficiency (LHE). Conversely, D2@TiO_2 and D5@TiO_2 are characterised by an optimal equilibrium state, combining good absorption with powerful regeneration. In conclusion, these results highlight the need for simultaneous molecular co-optimisation of absorption levels and frontier orbitals in order to advance the next generation of dye-sensitised solar cells.

References

1. Boro B., Gogoi B., Rajbongshi B.M., Ramchiary A. (**2018**) Nano-structured TiO_2/ZnO nanocomposite for dye-sensitized solar cells application: A review. *Renew. Sustain. Energy Rev.*, 81, 2264–2270. https://doi.org/10.1016/j.rser.2017.06.035

2. Dhorkule M., Lamrood P., Ralegankar S., Patole S.P., Wagh S.S., Pathan H.M. (**2024**) Unveiling the efficiency of dye-sensitized solar cells: a journey from synthetic to natural dyes. *ES Food Agrofor.*, 16(2), 1086. https://doi.org/10.30919/esfaf1086

3. Baxter J.B. (**2012**) Commercialization of dye-sensitized solar cells: present status and future research needs. *J. Vac. Sci. Technol. A*, 30, 020801. https://doi.org/10.1116/1.3676433

4. Joseph I., Louis H., Unimuke T.O., Etim I.S., Orosun M.M., Odey J. (**2020**) Overview of operational principles and advances of dye-sensitized solar cells. *Appl. Sol. Energy*, 56(5), 334–363. https://doi.org/10.3103/S0003701X20050072

5. Idris N.H., Cheong M., Kennedy K.Y., Ohno B.J.T., Lee H.L. (**2022**) Buoyant titanium dioxide as high-performance photocatalyst. *J. Environ. Chem. Eng.*, 10(3), 107549. https://doi.org/10.1016/j.jece.2022.107549

6. Sharma K., Vinay S., Sharma S.S. (**2018**) Dye-sensitized solar cells: fundamentals and current status. *Nanoscale Res. Lett.*, 13, 381. https://doi.org/10.1186/s11671-018-2760-6

7. Roohi H., Mohtamadifar N. (**2022**) Donor group and electron-accepting substitutions tuning D–π–A dyes. *RSC Adv.*, 12, 11557–11573. https://doi.org/10.1039/D2RA00906D

8. Wei T., Liu Y. (**2017**) Estimation of global rebound effect caused by energy efficiency improvement. *Energy Econ.*, 66, 27–34. https://doi.org/10.1016/j.eneco.2017.05.030

9. Elkabous M., Ouachekradi M., Sergent C., Karzazi Y. (**2025**) Electron transfer mechanism from D–π–A dyes to TiO_2 surface. *Adv. Mater. Sustain. Energy Eng.*, 125–142. https://doi.org/10.1007/978-3-031-75032-8_10

10. Drzewiecka-Matuszek A., Rutkowska-Zbik D. (**2021**) TD-DFT theory applied to porphyrinoid-based photosensitizers. *Molecules*, 26(23), 7176. https://doi.org/10.3390/molecules26237176

11. Chai J.–D., Head-Gordon M. (**2008**) Long-range corrected hybrid density functionals with dispersion corrections. *Phys. Chem. Chem. Phys.*, 10, 6615–6620. https://doi.org/10.1039/B810189B

12. Adamo C., Barone V. (**1998**) Exchange functionals with improved long-range behavior. *J. Chem. Phys.*, 108, 664–675. https://doi.org/10.1063/1.475428

13. Civalleri B., Zicovich-Wilson C.M., Valenzano L., Ugliengo P. (**2008**) B3LYP-D applied to molecular crystals. *CrystEngComm*, 10, 405–410. https://doi.org/10.1039/B715018K

14. Yanai T., Tew D.P., Handy N.C. (**2004**) CAM-B3LYP functional. *Chem. Phys. Lett.*, 393, 51–57. https://doi.org/10.1016/j.cplett.2004.06.011

15. Fei Z., Boufflet P., Wood S., et al. (**2015**) Fluorination effects in poly(thiophene)s. *J. Am. Chem. Soc.*, 137, 6866–6879. https://doi.org/10.1021/jacs.5b02785

16. Janjua M.R.S.A. (**2017**) Pi-spacer effects on small-molecule acceptors. *J. Clust. Sci.*, 28, 2419–2431. https://doi.org/10.1007/s10876-017-1233-x

17. Aboulouard A., Demir N., Can M., El Idrissi M. (**2023**) Quinoxaline derivatives as electron donor materials. *J. Mol. Graph. Model.*, 121, 108462. https://doi.org/10.1016/j.jmgm.2023.108462

18. Lee C.P., Lin R.Y.Y., Lin L.Y., et al. (**2015**) Progress in organic sensitizers for DSSCs. *RSC Adv.*, 5, 23810–23825. https://doi.org/10.1039/C4RA16493H

19. Diany R., Kerraj S., Aboulouard A., et al. (**2024**) Quinoxaline-based dyes for DSSCs. *J. Comput. Electron.*, 23, 1195–1208. https://doi.org/10.1007/s10825-024-02211-3

20. Chanana G., Batra K. (**2021**) Modelling of D–π–A dye molecules. *J. Mol. Model.*, 27, 229. https://doi.org/10.1007/s00894-021-04824-y

21. Aboulouard A., Atouailaa M.K., Elhadadi B., et al. (**2022**) Non-fullerene acceptors based on thiophene. *Mater. Today Proc.*, 66, 329–334. https://doi.org/10.1016/j.matpr.2022.05.426

22. Boukili B., Mennas I., Arif A., et al. (**2025**) TD-DFT screening of acrylic-based dyes. *Phys. Chem. Res.*, 13(3). https://doi.org/10.22036/pcr.2025.522084.2681

23. Gómez S., Giovannini T., Cappelli C. (**2020**) Absorption spectra of xanthines in solution. *Phys. Chem. Chem. Phys.*, 22, 5929–5941. https://doi.org/10.1039/C9CP05420K

24. Aboulouard A., Arif A., Can M., El Idrissi M. (**2024**) Quinoxaline-based NFAs engineering. *Mater. Chem. Phys.*, 310, 127993. https://doi.org/10.1016/j.matchemphys.2024.127993

25. Cacelli I., Prampolini G. (**2007**) Parametrization of force fields. *J. Chem. Theory Comput.*, 3, 1803–1817. https://doi.org/10.1021/ct700113h

26. Pérez J.F., Hadad C.Z., Restrepo A. (**2008**) Structural analysis of the water tetramer. *Int. J. Quantum Chem.*, 108, 1653–1659. https://doi.org/10.1002/qua.21615

27. Rawat P., Singh R.N. (**2014**) Reactivity of synthesized pyrrole derivatives. *J. Mol. Struct.*, 1074, 201–212. https://doi.org/10.1016/j.molstruc.2014.05.050

28. Afshari T., Mohsennia M. (**2019**) Diels–Alder reaction using MEDT. *J. Phys. Org. Chem.*, 32, e3937. https://doi.org/10.1002/poc.3937

29. Li S., Zhang Y., Xu Y., et al. (**2024**) Thienonaphthalimide NFAs. *Comput. Theor. Chem.*, 1240, 114832. https://doi.org/10.1016/j.comptc.2024.114832

30. Yu A.–Y., Efil K., Yang R., Hu Q.M. (**2015**) Properties of methyl bromide. *Z. Naturforsch. A*, 70, 1025–1030. https://doi.org/10.1515/zna-2015-0351
31. Abdellah I.M., Koraiem A.I., El-Shafei A. (**2019**) Ru(II) complexes for DSSCs. *Sol. Energy*, 177, 642–651. https://doi.org/10.1016/j.solener.2018.11.047
32. Kerraj S., Salah M., El Idrissi M., et al. (**2022**) Ru, Rh, Ir complexes for DSSCs. *Comput. Theor. Chem.*, 1209, 113630. https://doi.org/10.1016/j.comptc.2022.113630
33. Ryu S., Noh J.H., Jeon N.J., et al. (**2014**) Voltage output of perovskite solar cells. *Energy Environ. Sci.*, 7, 2614–2618. https://doi.org/10.1039/C4EE00762J
34. Zouitina S., Aboulouard A., El Ghazali A., El Idrissi M. (**2023**) Thiophene donors for BHJ solar cells. *J. Fluoresc.*, 33, 553–563. https://doi.org/10.1007/s10895-022-03077-z
35. Zhang J., Li H.–B., Sun S.–L., et al. (**2011**) Diarylamine–fluorene dyes for DSSCs. *J. Mater. Chem.*, 22, 568–576. https://doi.org/10.1039/C1JM13028E
36. Brédas J.–L., Beljonne D., Coropceanu V., Cornil J. (**2004**) Charge-transfer processes in conjugated systems. *Chem. Rev.*, 104, 4971–5004. https://doi.org/10.1021/cr040084k
37. Mehboob M.Y., Khan M.U., Hussain R., et al. (**2021**) BDT-based acceptors for OSCs. *Spectrochim. Acta A*, 244, 118873. https://doi.org/10.1016/j.saa.2020.118873
38. Delley B. (**2000**) DMol³ approach. *J. Chem. Phys.*, 113, 7756–7764. https://doi.org/10.1063/1.1316015
39. Perdew J.P. (**1996**) GGA made simple. *Phys. Rev. Lett.*, 77, 3865–3868. https://doi.org/10.1103/PhysRevLett.77.3865
40. Benedek N.A., Snook I.K., Latham K., Yarovsky I. (**2005**) Numerical basis sets in DFT. *J. Chem. Phys.*, 122, 144102. https://doi.org/10.1063/1.1876152
41. Zhang L., Zhang Y., Zhang L. (**2017**) Auxiliary acceptor tuning in D–A–π–A dyes. *Dyes Pigm.*, 139, 1–7. https://doi.org/10.1016/j.dyepig.2017.01.026
42. Chen H., Gong Y., Vázquez-Mayagoitia A., Cole J.M. (**2019**) Dye aggregation and binding modes. *ACS Appl. Energy Mater.*, 3, 423–430. https://doi.org/10.1021/acsaem.9b01666
43. Bakhite E.A., et al. (**2025**) Thienopyridines and related heterocycles as insecticides. *Russ. J. Bioorg. Chem.*, 51(2), 816–826. https://doi.org/10.1134/S1068162024605512
44. Khamies E., et al. (**2024**) Pyridine derivatives as insecticides. *J. Agric. Food Chem.*, 72, 20842–20849. https://doi.org/10.1021/acs.jafc.4c03947
45. El Gaby M.S.A., et al. (**2024**) Thiazole-hydrazone derivatives against *Spodoptera frugiperda*. *Russ. J. Bioorg. Chem.*, 50(3), 1037–1048. https://doi.org/10.1134/S1068162024030282
46. Gad M.A., et al. (**2025**) Pyridine-containing insecticidal compounds. *Curr. Chem. Lett.*, 14(3), 407–416.
47. Fouad M.R., et al. (**2024**) Fate and behavior of imidacloprid. *Environ. Sci. Pollut. Res.*, 31, 61345–61355. https://doi.org/10.1007/s11356-024-35178-6
48. Hassan K.M., et al. (**2024**) 2-Indolinone derivatives as anticancer agents. *Curr. Chem. Lett.*, 13(1), 241–254. https://doi.org/10.5267/j.ccl.2023.6.005
49. Aboulfotoh A., Mohamed G.G., El-Didamony A.M., El-Sadek M.M. (**2024**) Instrumental analytical techniques for evaluating anti-infective drugs in pharmaceutical products and biological fluids. *Curr. Chem. Lett.*, 13(3), 491–502. https://doi.org/10.5267/j.ccl.2023.12.004
50. Gad M.A., Ibrahim A.A., El-Sayed M.M., et al. (**2025**) Bioefficacy and docking of pyridine compounds. *Curr. Chem. Lett.*, 14, 407–416.
51. Fouad M.R., Ibrahim A.E., Ahmed M.M., et al. (**2024**) Environmental behavior of imidacloprid. *Environ. Sci. Pollut. Res.*, 31, 61345–61355. https://doi.org/10.1007/s11356-024-35178-6

© 2026 by the authors; licensee Growing Science, Canada. This is an open access article distributed under the terms and conditions of the Creative Commons Attribution (CC-BY) license (http://creativecommons.org/licenses/by/4.0/).